

On the maximal number of real embeddings of minimally rigid graphs in \mathbb{R}^2 , \mathbb{R}^3 and S^2

Evangelos Bartzos^{1,2}, Ioannis Emiris¹, Jan Legerský³, and Elias Tsigaridas⁴

¹Department of Informatics and Telecommunications, National Kapodistrian University of Athens

²ATHENA Research Center

³Research Institute for Symbolic Computation, Johannes Kepler University, Linz

⁴Sorbonne Université, CNRS, INRIA, Laboratoire d'Informatique de Paris 6 (LIP6), Équipe POLSYS

Abstract

Rigidity theory studies the properties of graphs that can have rigid embeddings in a euclidean space \mathbb{R}^d or on a sphere and which in addition satisfy certain edge length constraints. One of the major open problems in this field is to determine lower and upper bounds on the number of realizations with respect to a given number of vertices. This problem is closely related to the classification of rigid graphs according to their maximal number of real embeddings.

In this paper, we are interested in finding edge lengths that can maximize the number of real embeddings of minimally rigid graphs in the plane, space, and on the sphere. We use algebraic formulations to provide upper bounds. To find values of the parameters that lead to graphs with a large number of real realizations, possibly attaining the (algebraic) upper bounds, we use some standard heuristics and we also develop a new method inspired by coupler curves. We apply this new method to obtain embeddings in \mathbb{R}^3 . One of its main novelties is that it allows us to sample efficiently from a larger number of parameters by selecting only a subset of them at each iteration.

Our results include a full classification of the 7-vertex graphs according to their maximal numbers of real embeddings in the cases of the embeddings in \mathbb{R}^2 and \mathbb{R}^3 , while in the case of S^2 we achieve this classification for all 6-vertex graphs. Additionally, by increasing the number of embeddings of selected graphs, we improve the previously known asymptotic lower bound on the maximum number of realizations. The methods and the results concerning the spatial embeddings are part of the proceedings of ISSAC 2018 [[1]].

1 Introduction

Rigidity theory is a very wide area of mathematical research that combines elements of graph theory and algebraic geometry. The numerous applications of rigid graphs in other domains, such as robotics [16, 33, 35], structural bioinformatics [13, 23], sensor network localization [36] and architecture [15], give additional motivation to find efficient algorithms to compute them and classify their properties. One of the open problems in rigidity theory is to determine bounds on the maximal number of real embeddings of rigid graphs. We are interested in improving the currently known bounds.

An embedding of a simple graph $G = (V, E)$ in a euclidean space \mathbb{R}^d is a map from the set V to \mathbb{R}^d . We require that it satisfies certain edge constraints, namely, the distance between the images of any two adjacent vertices equals a given edge length. Let $\mathbf{p} = (p_1, p_2, \dots, p_n)$ be a configuration of $n = |V|$ points in \mathbb{R}^d and $\boldsymbol{\lambda} = (\|p_i - p_j\|)_{ij \in E}$ be the vector of edge lengths induced by \mathbf{p} . The graph G with edge lengths $\boldsymbol{\lambda}$ is called *rigid* in \mathbb{R}^d if the number of embeddings in \mathbb{R}^d having the same edge lengths is finite modulo rigid motions. The graph G is *generically rigid* in \mathbb{R}^d iff it is rigid in \mathbb{R}^d for edge lengths induced by any generic configuration. Additionally, if G is *generically rigid* and removing any edge $e \in E$ yields a non-rigid graph $G - e$, then G is called *generically minimally rigid* in \mathbb{R}^d .

In the first half of the 20th century, [27, 26] made notable progress on understanding the properties of minimally rigid graphs, but her work was forgotten. [22] rediscovered that we can fully characterize the minimally rigid graphs in \mathbb{R}^2 using the edge count property [24]. Since then, these graphs are known as *Laman graphs*. In honor of Hilda Pollaczek-Geiringer, we have chosen to call minimally rigid graphs in \mathbb{R}^3 *Geiringer graphs*, as in [18]. Rigidity is defined also on spheres [34]. In the case of S^2 , the edge count property of Laman graphs holds for minimally rigid graphs, while the distance from the origin poses an additional constraint.

Generically minimally rigid graphs are of great interest since they correspond to well-constrained algebraic systems. Given a rigid graph $G = (V, E)$ in \mathbb{R}^d and edge lengths $\boldsymbol{\lambda} = \{\lambda_{ij}\}_{ij \in E} \in \mathbb{R}_+^{|E|}$, we denote by $r_d(G, \boldsymbol{\lambda})$ the number of embeddings of G in \mathbb{R}^d , which are the real solutions of the corresponding algebraic systems. Let $r_d(G)$ denote the maximal number of real embeddings among all the choices of $\boldsymbol{\lambda}$ that yield a rigid conformation, i.e., when $r_d(G, \boldsymbol{\lambda})$ is finite. The total number of solutions of the corresponding algebraic system in \mathbb{C}^d is the number of complex embeddings of a graph. This gives a natural upper bound for $r_d(G)$ and is denoted by $c_d(G)$. Finally, we write $c_d(n)$ and $r_d(n)$ for the maximal number of complex and real embeddings, respectively, among all n -vertex rigid graphs in \mathbb{C}^d . We will also use the notation $r_{S^2}(G, \boldsymbol{\lambda})$, $r_{S^2}(G)$ and $c_{S^2}(G)$ for the real and complex number of embeddings on S^2 .

We can use lower and upper bounds on $r_d(G)$ to establish lower and upper bounds on $r_d(n)$ by gluing mechanisms in certain ways [7, 18].

Previous results Asymptotic upper bounds for $r_d(n)$ were computed as complex bounds of the determinantal variety of the distance matrix in [6, 7], while mixed volume techniques were applied in the case $d = 2$ in [30]. Both bounds behave asymptotically as $\mathcal{O}(2^{dn})$, which is considered as a rather loose bound. Tighter bounds for specific classes of Laman graphs can be found in [21].

Graph-specific approaches have been also used to compute bounds of graph embeddings in \mathbb{R}^2 and \mathbb{R}^3 . Mixed volume techniques [14] and a recent combinatorial algorithm for Laman graphs [8] have treated the complex case. In [7], it is proven that $r_2(6) = 24$ using coupler curves and some advanced stochastic methods are applied to show that $r_2(7) = 56$ in [12]. The latter yields 2.3003^n as a lower bound on maximal number of embeddings for Laman graphs; we improve this bound. The best known lower bound for $r_3(n)$ is 2.51984^n [14]; we also improve this bound. In general, the maximal number of real embeddings both in $d = 2$ and $d = 3$ for graphs with $n \leq 6$ vertices is known.

The main question is whether we can specify edge lengths that maximize the number of real embeddings. This question is related to more general open problems in real algebraic geometry concerning possible gaps between the number of complex and real solutions of an algebraic system depending on its parameters. There exist some upper [29] and lower [3, 4] bounds on the number of real positive roots, which take advantage of the structure of polynomials. Regarding applied cases, there is also the famous example on the maximization of the number of real Stewart-Gough Platform configurations [11], using a gradient descent method.

Our contribution We extend the existing results on the maximal number of real embeddings of Laman and Geiringer graphs. We provide bounds in the previously untreated case of spherical embeddings. In both cases, we have constructed all minimally rigid graphs using the methods described in [18] and we classify them according to the last Henneberg step. Subsequently, we use different systems to model our problem algebraically and we compute upper bounds for all computationally feasible cases. Since our main goal is to maximize the number of real embeddings, we specify the edge lengths in each case using certain heuristics.

In the ISSAC 2018 version we have treated the case of Geiringer graphs. We have developed a new method inspired by coupler curves that can search efficiently huge parametric spaces combining local and global sampling. An open-source implementation of our method is available in [2]. This implementation uses the polyhedral homotopy solver PHCpack [32] to find the solutions of algebraic systems. We are not aware of any other similar method. The method gave the maximal numbers of real embeddings of all 7-vertex Geiringer graphs and improved the existing lower maximal bound from 2.51984^n to 2.6390^n using selected 8-vertex graphs [1].

Besides the results announced in ISSAC 2018, we also improve the existing lower bounds on the number of real embeddings of selected Laman graphs on the plane and sphere. In these cases, we use some standard sampling methods to find parameters that maximize the number of embeddings. Our results give the maximal numbers of real embeddings of all 6-vertex and 7-vertex Laman graphs in S^2 and \mathbb{R}^2 respectively. We also specify parameters for larger graphs (up to 10 vertices for the embeddings on the plane and up to 8 vertices for spherical embeddings). These computations improve the existing lower bound on the maximal number of real embeddings from 2.3003^n to 2.3811^n for $d = 2$, while they establish 2.51984^n as a lower bound for the number of embeddings in S^2 .

Organization We organize the paper as follows: in Section 2, we give a brief introduction on rigidity theory and we describe the algebraic modeling in hand. In Section 3, we present the sampling methods that we use. Here we describe the method for maximizing the number of real embeddings of Geiringer graphs that is inspired by coupler curves. It previously appeared in [1]. In Section 4, we present our results in $d = 2$, S^2 , and $d = 3$. We derive a new lower bound on the maximal number of real embeddings for the first two cases and we restate the lower bound appeared in the proceedings of ISSAC 2018 for the spatial embeddings. In Section 5, we present an overview of our results and some future research problems.

2 Rigidity and Algebraic Modeling

First, we present some standard results about minimally rigid graphs (Sec. 2.1). We subsequently introduce the algebraic formulations we use to establish upper and lower bounds on the number of embeddings. In Sec. 2.2, we present a variation of the squared distance equations between adjacent vertices, while in Sec. 2.3 we apply the Cayley-Menger embeddability conditions.

2.1 Rigidity and Henneberg steps

Minimally rigid graphs correspond to well-constrained algebraic systems. The following theorem provides the total number of constraints for a minimally rigid graph and an upper bound on the number of edges of each subgraph (implying that no subsystem is over-constrained).

Theorem 1 ([24]). *If $G = (V, E)$ is a minimally rigid graph in \mathbb{R}^d , then the total number of edges is $|E| = d|V| - \binom{d+1}{2}$. Additionally, for each subgraph $G' = (V', E') \subset G$, the inequality $|E'| \leq d|V'| - \binom{d+1}{2}$ holds.*

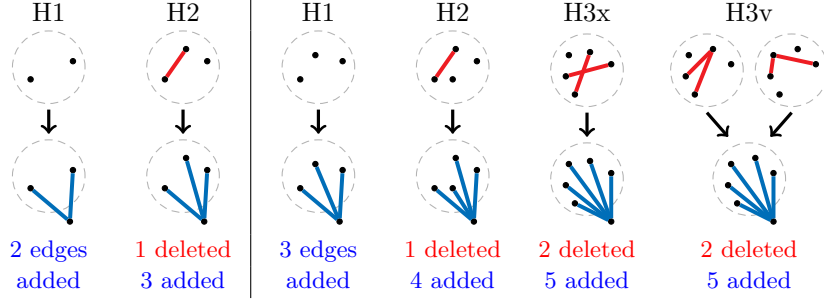


Figure 1: Henneberg steps in \mathbb{R}^2 (left) and \mathbb{R}^3 (right)

This condition is also sufficient for $d = 2$ and the set of these graphs coincide with Henneberg constructions starting from a single edge [22, 26, 27]. On the other hand, there are counterexamples in higher dimensions. This leads to one of the most important open questions in rigidity theory, that is the quest for a combinatorial characterization of minimally rigid graphs in dimension $d \geq 3$ [28]. Despite this fact, we know that using (extended) Henneberg steps we can construct a superset of minimally rigid graphs in all dimensions.

There are two Henneberg operations that preserve minimal rigidity in any dimension, see Fig. 1 [31]. The first move consists of adding a new vertex of degree d connecting it with d existing vertices. This step is known as Henneberg step I (H1) or vertex addition step. The second move consists of deleting an existing edge, then connecting a new vertex with the vertices of the deleted edges and $d - 1$ other existing vertices. This step is known as Henneberg step II (H2) or edge split step.

H1 and H2 steps are equivalent to the edge count property of Theorem 1 in $d = 2$, so they characterize Laman graphs completely. On the other hand, for $d = 3$, two extra steps are required to construct a superset of Geiringer graphs. They are known as Henneberg III (H3) or extended Henneberg steps. The graphs whose construction requires an H3 move have $n \geq 12$ vertices and they are out of the scope of this paper due to computational constraints.

Laman graphs can be embedded also on the sphere S^2 . In that case, we need to add an additional constraint, which is the distance between the center of the sphere and the vertices. This means that spherical n -vertex minimally rigid graphs could be seen as minimally rigid graphs in \mathbb{R}^3 with $n + 1$ vertices, one of which has degree n [34].

Let us notice that if there is a way to construct a graph G_{n+1} by applying an H1 move to G_n , then the number of embeddings is doubled, i.e., $c_d(G_{n+1}) = 2c_d(G_n)$ and $r_d(G_{n+1}) = 2r_d(G_n)$. On the other hand, experiments show that the effect of other Henneberg steps on the number of embeddings varies significantly depending on a graph [18]. Therefore, we classify the minimally rigid graphs according to the possible last Henneberg moves. This can be translated into a minimum degree condition, since if there is a vertex of degree d , then the graph can be constructed by an H1 move in the last step. We consider the graphs with at least one vertex of degree d as graphs, whose number of embeddings can be trivially obtained from a smaller graph, and we will use the term *H1-last* for them. We will also use the term *H2-last* for graphs with all vertices of degree at least $d + 1$.

2.2 Equations of spheres

In this section we define a set of equations to compute the embeddings of a graph. The equations are of two kinds. The first one corresponds to the squared distance between adjacent vertices. Although this set of *edge equations* suffices to find the embeddings of a graph, the mixed volume of this system is much bigger than the actual number of complex embeddings. This is not favorable for homotopy continuation polynomial solvers, which give us the fastest method to compute the embeddings. In order to overcome this problem, we use the *magnitude equations* that introduce new variables as the distance of each vertex from the origin [30, 14]. In that way, mixed volume can be significantly lowered.

Definition 1. Let $G = (V, E)$ be a graph with given edge lengths $\lambda = (\lambda_e)_{e \in E} \in \mathbb{R}_+^{|E|}$ and $X_u = (x_{u1}, x_{u2}, \dots, x_{ud})$ be the variables assigned to the coordinates of each vertex. If the graph contains a complete subgraph with d vertices v_1, v_2, \dots, v_d , then we can choose the coordinates of this d -simplex in a way that they satisfy the edge lengths of this subgraph. We define $S(G, \lambda, [v_1, v_2, \dots, v_d]) \subset \mathbb{C}^{d \cdot |V|}$ as the solutions of the following equations

$$\begin{aligned} \|X_u\|^2 - s_u &= 0 \quad \forall u \in V, \\ s_u + s_v - 2\langle X_u, X_v \rangle - \lambda_{uv}^2 &= 0 \quad \forall uv \in E, \end{aligned}$$

such that the d -simplex is fixed. We denote the real solutions $S(G, \lambda, [v_1, v_2, \dots, v_d]) \cap \mathbb{R}^{d \cdot |V|}$ by $S_{\mathbb{R}}(G, \lambda, [v_1, v_2, \dots, v_d])$.

Fixing the coordinates of the d -simplex, rotations and translations are removed from the set of solutions yielding a 0-dimensional system. In the case of Laman graphs, we fix v_1 in the origin and v_2 in the y -axis with coordinates $(0, \lambda_{1,2})$. In the case of Geiringer graphs, we fix again v_1 in the origin and v_2 in the y -axis with coordinates $(0, \lambda_{1,2}, 0)$. The vertex v_3 is on the plane $z = 0$, with $z_3 \geq 0$. Finally, in the case of spherical embeddings, we consider the extension to a Geiringer graph and we use the analogous equations fixing 2 points on $(0, 0, 1)$ and $(0, \sqrt{(1 - \cos(\theta_{1,2})^2)}, \cos(\theta_{1,2}))$, where $\theta_{1,2}$ is the angle between the vector of v_1 and v_2 .

The edge equations express the geometrical constraints of the graph, while the magnitude equations are used to avoid roots at toric infinity, resulting to tighter mixed volume [14, 30]. At this point we should remark that the mixed volume of sphere equations depends on the choice of the fixed d -simplex, so we computed all possible combinations to get the tightest bound.

We should also comment that $|S(G, \lambda, [v_1, v_2, \dots, v_d])|$ coincides with $c_d(G)$ for a generic choice of lengths λ and that $r_d(G, \lambda) = |S_{\mathbb{R}}(G, \lambda, [v_1, v_2, \dots, v_d])|$ for arbitrary λ .

2.3 Distance systems

A Cayley-Menger matrix is the matrix of squared distances extended by a row and column of ones (except for the diagonal which is always zero):

$$CM = \begin{pmatrix} 0 & 1 & 1 & \cdots & 1 \\ 1 & 0 & \lambda_{12}^2 & \cdots & \lambda_{1n}^2 \\ 1 & \lambda_{12}^2 & 0 & \ddots & \cdots \\ \cdots & \cdots & \ddots & \ddots & \cdots \\ 1 & \lambda_{1n}^2 & \lambda_{2n}^2 & \cdots & 0 \end{pmatrix},$$

where λ_{ij} is the distance between point i and j .

A fundamental result in distance geometry indicates the following embeddability condition [5]:

Theorem 2. *The squared distances of a CM matrix can be embedded in \mathbb{R}^d iff*

- $\text{rank}(CM) = d + 2$
- $(-1)^k \det(CM') \geq 0$, for every submatrix CM' with size $k + 1 \leq d + 2$ that includes the extending row/column.

In the case of graph embeddings, each known entry corresponds to a squared edge length, while the variables correspond to unknown edge lengths. Any solution of the semi-algebraic system is an embedding of the graph in \mathbb{R}^d up to isometries. Considering only the solutions of the determinantal variety, we get the complex embeddings of the graph. The set of inequalities correspond to certain geometrical constraints on the edge lengths, such as positivity and triangular inequalities in dimension 2. In dimension 3, *tetrahedral inequalities* (which are a generalization of triangular inequalities on the area of the triangles of a tetrahedron) should be also satisfied [10].

The systems of equations of determinantal varieties are overconstrained. For example, there are 35 equations in 10 variables for 7-vertex Laman graphs, while for 7-vertex Geiringer graphs, there are 21 equations in 6 variables. Despite this fact, it is possible to find zero-dimensional square subsystems of these systems of equations [14, 12]. Notice that the zero set of the whole determinantal variety corresponds to the missing edge lengths of the complete graph. This means that the solutions of the subsystem correspond to a superset of the missing edge lengths. If the graph extended by the edges corresponding to the variables of the subsystem is *globally rigid* (a rigid graph with a unique embedding up to isometries), then the subsystem gives an upper bound on the number of embeddings of the whole graph [20]. In dimension 2 there is a combinatorial characterization for globally rigid graphs [9], while for arbitrary dimension we can check it using the rank of stress matrices of rigidity matroids [17].

In our research, it was easy to detect square subsystems, if no restriction was imposed on the number of variables. The point was to find the optimal ones in the sense that they would be 0-dimensional and serve to find the embeddings of a graph (so they should have exactly the same number of complex solutions as the whole variety) or a useful upper bound. Throughout our experiments, we found out that subsystems with $n - (d + 1)$ equations can meet this requirements. Additionally, the following lemma shows that for $d = 2$ and $d = 3$, there is always an extension of a minimally rigid graph with $n - (d + 1)$ edges that results to a globally rigid graph (the version of this lemma for $d = 3$ appears also in [1]).

Lemma 1. *For every minimally rigid graph $G = (V, E)$ in dimensions $d = 2$ and $d = 3$, there is at least one extended graph $H = G \cup \{e_1, e_2, \dots, e_k\}$, with $k = n - (d + 1)$ and $e_i \notin E$, which is globally rigid in \mathbb{C}^d .*

Proof. The only 4-vertex minimally rigid graph in dimension 2 (resp. 5-vertex in dimension 3) is obtained by applying an H1 step to the triangle (resp. tetrahedron in dimension 3). If we extend this graph with the only non-existing edge, we obtain a complete graph, so the lemma holds. Let the lemma hold for all graphs with n or less vertices. H2 steps are known to preserve global rigidity [9]. So we need to prove the lemma for H1 steps in both dimensions and H3 steps in dimension 3.

Let a Laman graph G_{n+1} be constructed by an H1 move applied to an n -vertex graph G_n , whose extended globally rigid graph is H_n . Without loss of generality, this move connects a new vertex v_{n+1} with vertices v_1, v_2 . Let u be a neighbour of v_1 in G_{n+1} not such that $v_2 \neq u$. The edge uv_1 exists also in G_n and H_n . If we set $H'_{n+1} = (H_n \cup \{v_1v_{n+1}, v_2v_{n+1}, uv_{n+1}\}) - \{v_1u\}$, then H'_{n+1} is globally rigid, because it is constructed from H_n by an H2 step. Hence, $H_{n+1} = H'_{n+1} \cup \{uv_1\}$ is also globally rigid, proving the statement in the case of H1 steps in dimension 2. The same result holds in arbitrary dimension (see Figure 2 for $d = 3$).

Both H3 steps consist of an H2 step followed by a second edge deletion in the existing graph and a new connection with v_{n+1} . So, if we apply an H3 move in H_n and subsequently add the second deleted edge, then H_{n+1} is globally rigid. \square

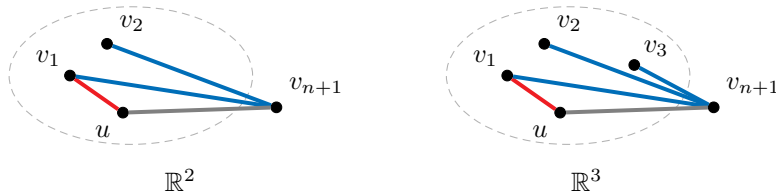


Figure 2: H_{n+1} is constructed by an H1 step applied to H_n (blue edges), extended with the edge uv_{n+1} . This is equivalent with applying an H2 step and adding the deleted edge uv_{n+1} .

Although we proved that there are always globally rigid extensions with $n - (d + 1)$ supplementary edges, it is not always possible to find a Cayley-Menger subvariety corresponding to them. We could detect such subsystems for all graphs with $n \leq 7$ vertices in both dimensions, but there exist bigger graphs for which this property does not hold.

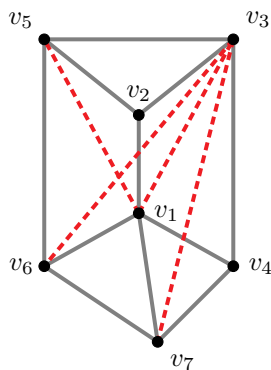


Figure 3: The embeddings of the Laman graph L_{48H2} (grey edges) can be represented by submatrices of $CM_{L_{48H2}}$ that involve only variables corresponding to the 4 red dashed edges. The extended graph is globally rigid. This construction can be used to find also the spherical embeddings of L_{48} .

We will give some representative examples of optimal CM subsystems in the cases of Laman, Geiringer and spherical graphs. For instance, L_{48H2} is a 7-vertex Laman graph (see Figure 3), which has $c_2(L_{48H2}) = r_2(L_{48H2}) = 48$ and $c_{S^2}(L_{48H2}) = r_{S^2}(L_{48H2}) = 64$ (See Section 4). There are 11 subsystems of this CM variety in 4 variables, which all have exactly the same number of solutions. In the following CM matrix, we present one of these choices involving the

variables x_1, x_2, x_6 and x_7 .

$$CM_{L_{48H2}} = \begin{pmatrix} 0 & 1 & 1 & 1 & 1 & 1 & 1 & 1 \\ 1 & 0 & \lambda_{12}^2 & \textcolor{red}{x}_1 & \lambda_{14}^2 & \textcolor{red}{x}_2 & \lambda_{16}^2 & \lambda_{17}^2 \\ 1 & \lambda_{12}^2 & 0 & \lambda_{23}^2 & \textcolor{blue}{x}_3 & \lambda_{25}^2 & \textcolor{blue}{x}_4 & \textcolor{blue}{x}_5 \\ 1 & \textcolor{red}{x}_1 & \lambda_{23}^2 & 0 & \lambda_{34}^2 & \lambda_{35}^2 & \textcolor{red}{x}_6 & \textcolor{red}{x}_7 \\ 1 & \lambda_{14}^2 & \textcolor{blue}{x}_3 & \lambda_{34}^2 & 0 & \textcolor{blue}{x}_8 & \textcolor{blue}{x}_9 & \lambda_{47}^2 \\ 1 & \textcolor{red}{x}_2 & \lambda_{25}^2 & \lambda_{35}^2 & \textcolor{blue}{x}_8 & 0 & \lambda_{56}^2 & \textcolor{blue}{x}_{10} \\ 1 & \lambda_{16}^2 & \textcolor{blue}{x}_4 & \textcolor{red}{x}_6 & \textcolor{blue}{x}_9 & \lambda_{56}^2 & 0 & \lambda_{67} \\ 1 & \lambda_{17}^2 & \textcolor{blue}{x}_5 & \textcolor{red}{x}_7 & \lambda_{47}^2 & \textcolor{blue}{x}_{10} & \lambda_{67} & 0 \end{pmatrix}$$

In order to compute the number of real embeddings, we need to find the semi-algebraic set containing the positive solutions of this system that satisfy the triangular inequalities.

We can use the same extended graph to compute the spherical embeddings of L_{48H2} . An additional constraint is needed in that case, which represents the distance from the origin, as a new column and row with ones. The determinantal subsystem is derived from the rank condition of 3-dimensional embeddings. Elementary matrix operations can lead to a formulation that considers the cosines of the angles between two points as matrix entries, denoted as c_{ij} .

$$CM_{S^2(L_{48H2})} = \begin{pmatrix} 0 & 1 & 1 & 1 & 1 & 1 & 1 & 1 & 1 \\ 1 & 0 & \lambda_{12}^2 & \textcolor{red}{x}_1 & \lambda_{14}^2 & \textcolor{red}{x}_2 & \lambda_{16}^2 & \lambda_{17}^2 & 1 \\ 1 & \lambda_{12}^2 & 0 & \lambda_{23}^2 & \textcolor{blue}{x}_3 & \lambda_{25}^2 & \textcolor{blue}{x}_4 & \textcolor{blue}{x}_5 & 1 \\ 1 & \textcolor{red}{x}_1 & \lambda_{23}^2 & 0 & \lambda_{34}^2 & \lambda_{35}^2 & \textcolor{red}{x}_6 & \textcolor{red}{x}_7 & 1 \\ 1 & \lambda_{14}^2 & \textcolor{blue}{x}_3 & \lambda_{34}^2 & 0 & \textcolor{blue}{x}_8 & \textcolor{blue}{x}_9 & \lambda_{47}^2 & 1 \\ 1 & \textcolor{red}{x}_2 & \lambda_{25}^2 & \lambda_{35}^2 & \textcolor{blue}{x}_8 & 0 & \lambda_{56}^2 & \textcolor{blue}{x}_{10} & 1 \\ 1 & \lambda_{16}^2 & \textcolor{blue}{x}_4 & \textcolor{red}{x}_6 & \textcolor{blue}{x}_9 & \lambda_{56}^2 & 0 & \lambda_{67} & 1 \\ 1 & \lambda_{17}^2 & \textcolor{blue}{x}_5 & \textcolor{red}{x}_7 & \lambda_{47}^2 & \textcolor{blue}{x}_{10} & \lambda_{67} & 0 & 1 \\ 1 & 1 & 1 & 1 & 1 & 1 & 1 & 1 & 0 \end{pmatrix} \\ \sim \begin{pmatrix} 0 & 1 & 1 & 1 & 1 & 1 & 1 & 1 & 2 \\ 1 & 0 & c_{12} & \textcolor{red}{y}_1 & c_{14} & \textcolor{red}{y}_2 & c_{16} & c_{17} & 1 \\ 1 & c_{12} & 0 & c_{23} & \textcolor{blue}{y}_3 & c_{25} & \textcolor{blue}{y}_4 & \textcolor{blue}{y}_5 & 1 \\ 1 & \textcolor{red}{y}_1 & c_{23} & 0 & c_{34} & c_{35} & \textcolor{red}{y}_6 & \textcolor{red}{y}_7 & 1 \\ 1 & c_{14} & \textcolor{blue}{y}_3 & c_{34} & 0 & \textcolor{blue}{y}_8 & \textcolor{blue}{y}_9 & c_{47} & 1 \\ 1 & \textcolor{red}{y}_2 & c_{25} & c_{35} & \textcolor{blue}{y}_8 & 0 & c_{56} & \textcolor{blue}{y}_{10} & 1 \\ 1 & c_{16} & \textcolor{blue}{y}_4 & \textcolor{red}{y}_6 & \textcolor{blue}{y}_9 & c_{56} & 0 & c_{67} & 1 \\ 1 & c_{17} & \textcolor{blue}{y}_5 & \textcolor{red}{y}_7 & c_{47} & \textcolor{blue}{y}_{10} & c_{67} & 0 & 1 \\ -2 & 1 & 1 & 1 & 1 & 1 & 1 & 1 & 0 \end{pmatrix}$$

The semi-algebraic conditions of the latter formulation, requires that any solution of the determinantal subsystem lies in the interval $[-1, 1]$ and that the triangular inequalities on the sphere are satisfied. The second is equivalent to the positivity of $2c_{ij}c_{ik}c_{jk} - c_{ij}^2 - c_{ik}^2 - c_{jk}^2 + 1$ for 3 points i, j, k on the sphere, where c_{ij} is the cosine of the angle between points i and j and can be obtained as the determinant of a 5x5 submatrix containing both columns and rows with ones.

We take the graph G_{48} , see Figure 4 as an example of CM subvarieties of Geiringer graphs (which was also used in [1]). The graph G_{48} has the maximal number of embeddings among all 7-vertex Geiringer graphs ($c_3(G_{48}) = r_3(G_{48}) = 48$, see Section 4). There are 5 different square systems in 3 variables that completely define the embeddings. We can choose one of them

involving only x_1, x_2, x_3 :

$$CM_{G_{48}} = \begin{pmatrix} 0 & 1 & 1 & 1 & 1 & 1 & 1 & 1 \\ 1 & 0 & \lambda_{12}^2 & \lambda_{13}^2 & \lambda_{14}^2 & \lambda_{15}^2 & \lambda_{16}^2 & \textcolor{red}{x}_1 \\ 1 & \lambda_{21}^2 & 0 & \lambda_{23}^2 & \textcolor{red}{x}_2 & \textcolor{red}{x}_3 & \lambda_{26}^2 & \lambda_{27}^2 \\ 1 & \lambda_{31}^2 & \lambda_{32}^2 & 0 & \lambda_{34}^2 & \textcolor{blue}{x}_4 & \textcolor{blue}{x}_5 & \lambda_{37}^2 \\ 1 & \lambda_{41}^2 & \textcolor{red}{x}_2 & \lambda_{43}^2 & 0 & \lambda_{45}^2 & \textcolor{blue}{x}_6 & \lambda_{47}^2 \\ 1 & \lambda_{51}^2 & \textcolor{red}{x}_3 & \textcolor{blue}{x}_4 & \lambda_{54}^2 & 0 & \lambda_{56}^2 & \lambda_{57}^2 \\ 1 & \lambda_{61}^2 & \lambda_{62}^2 & \textcolor{blue}{x}_5 & \textcolor{blue}{x}_6 & \lambda_{65}^2 & 0 & \lambda_{67}^2 \\ 1 & \textcolor{red}{x}_1 & \lambda_{72}^2 & \lambda_{73}^2 & \lambda_{74}^2 & \lambda_{75}^2 & \lambda_{76}^2 & 0 \end{pmatrix}$$

The set of real embeddings in that case is given by the solutions of the subsystem that satisfy positivity, triangular and tetragonal inequalities.

Extending this graph with the edge v_1v_7 suffices for global rigidity. This edge corresponds to the variable x_1 and it is possible to get a single equation by applying resultants in the 3x3 system of determinantal equations (see Figure 4).

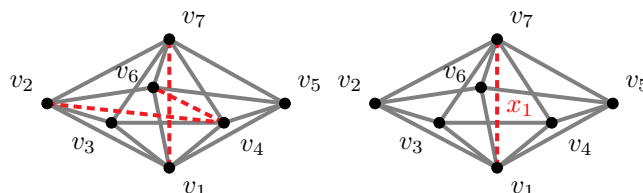


Figure 4: The graph G_{48} (grey edges). There are submatrices of $CM_{G_{48}}$ that involve only variables corresponding to the 3 red dashed edges of the left graph. The graph G_{48} extended by the edge v_1v_7 (that corresponds to the variable x_1) is globally rigid.

Since a single edge is needed to find the whole embedding, we can use only the inequalities involving only this variable (5 triangular and 5 tetragonal inequalities instead of 35 that involve all variables).

3 Increasing the number of real embeddings

Our main goal throughout our experiments was to find the parameters that can maximize the number of real embeddings of minimally rigid graphs. One open problem in rigidity theory is whether the maximal number of real embeddings of a given graph can be the same as the number of complex embeddings. Although there exists an 8-vertex Laman graph for which it has been proven that $r_2(G) < c_2(G)$ [20], in most cases we consider the number of complex embeddings as the upper bound we try to reach. In our research, we were mostly concentrated on the cases of graphs with the biggest number of complex embeddings, among all other minimally rigid graphs with the same number of vertices.

Additionally to some standard sampling methods, we developed a new method that can increase efficiently the number of real embeddings for certain Geiringer graphs, which was initially introduced in ISSAC 2018. Our method is inspired by coupler curves approach and uses G_{48}

as a model. Taking advantage of our implementation based on this technique, we were able to increase lower bounds on $r_3(G)$ for many graphs and establish new asymptotic lower bounds on the maximal number of embeddings of Geiringer graphs.

3.1 Standard sampling methods

Finding initial configurations We applied different heuristics to find initial configurations for our parameter sampling. First of all, we tried to compute the number of real embeddings of totally random configurations. This resulted in finding maximal numbers of real embeddings for graphs with $c_d(G) = 2^{n-(d+1)}$. For example, it took less than 20 minutes to detect parameters that attain the maximum for all 8-vertex H2-last Geiringer graphs with $c_3(G) = 32$.

We also used almost degenerate locus as starting points. In order to increase $r_2(G)$ of Laman graphs with maximal numbers of complex embeddings w.r.t. a given number of vertices, we chose lengths very close to the unit length. Similarly, in the case of Geiringer graphs, we perturbed degenerate conformations. For example, in order to find an initial point for G_{48} , we separate the edges into three sets with edge lengths being the same in each of them: the *ring edges* of the 5-cycle, the *top edges* that connect v_7 with the ring and the *bottom edges* that connect v_1 with the ring — see Figure 4. We subsequently found edge lengths that maximized the intervals imposed by triangular and tetragonal inequalities up to scaling and we perturbed the resulting lengths.

Finally, we also used as starting points conformations of smaller graphs with maximal numbers of embeddings. For instance, gluing v_7 and v_8 in G_{160} results in G_{48} . Perturbing a labeling λ of G_{48} such that $r_3(G_{48}, \lambda) = 48$, we could get a starting point for the sampling of G_{160} that would result in a big number of real embeddings.

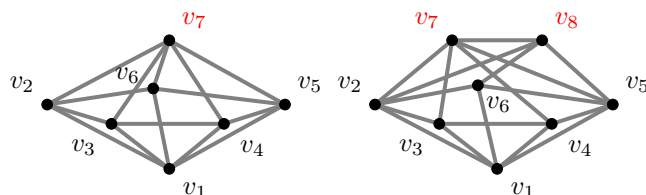


Figure 5: Coinciding vertices v_7 and v_8 of G_{160} results in G_{48} .

Stochastic methods We have used stochastic methods for different graphs in order to increase the number of embeddings. Our method uses a variant of the tools suggested in [12]. We penalize the loss of real roots and the increase of the imaginary part of complex solutions to decide if the resulted labeling constitutes a new starting point. This method could increase the number of embeddings, but rarely attained the maximum.

Parametric searching with CAD method The methods described in the previous paragraph are local methods. In order to search globally one parameter, we used Maple's subpackage `RootFinding` [Parametric] in Maple18. This package is an implementation of Cylindrical Algebraic Decomposition principles for semi-algebraic sets. The input consists of the equations and the inequalities of the system and the list of variables separating them from parameters. The

output is a cell decomposition of the space of parameters according to the number of solutions of the semi-algebraic conditions.

In our problem, we were able to take advantage of this implementation using distance systems of 7-vertex graphs and searching for only one parameter. Sphere equations failed to give any result, while computational constraints did not let us search two or more parameters simultaneously.

In [1] we use this sampling method to increase the number of real embeddings of G_{48} . This sampling was also used to increase the number of spherical and planar embeddings of Laman graphs with 7 vertices. In some situations it was even possible to attend the maximal number of embeddings for a given graph.

3.2 Coupler curve

The previous methods fail to attain tight bounds for Geiringer graphs with maximal number of embeddings efficiently. For example, using CAD, we could find 28 real embeddings for G_{48} , but it seems impossible to increase this number by local searching in all parameters or global sampling only one of them. Thus, we developed a new method that samples only subset of edge lengths in every iteration. This procedure is motivated by visualization of coupler curves. We remark that we already presented this method at ISSAC'18.

Let $G = (V, E)$ be a minimally rigid graph with a triangle and an edge uc . If $H = (V, E \setminus uc)$ is obtained from G by removing the edge uc , then the set of embeddings satisfying the constraints given by generic edge lengths and fixing the triangle is 1-dimensional. The projection of this curve to the coordinates of the vertex c is a so called *coupler curve*. [7] used this idea for proving that the Desargues (3-prism) graph has 24 real embeddings in \mathbb{R}^2 . Namely, they found edge lengths such there are 24 intersections of the coupler curve with a circle representing the removed edge. This approach can be clearly extended into \mathbb{R}^3 — the number of embeddings of G is the same as the number of intersection of the coupler curve of c with the sphere centered at u with a radius λ_{uc} . Now, we define specifically a coupler curve in \mathbb{R}^3 .

Definition 2. Let H be a graph with edge lengths $\lambda = (\lambda_e)_{e \in E_H}$ and $v_1, v_2, v_3 \in V_H$ be such that $v_1v_2, v_2v_3, v_1v_3 \in E_H$. If the set $S_{\mathbb{R}}(H, \lambda, [v_1, v_2, v_3])$ is one dimensional and $c \in V_H$, then the set

$$\mathcal{C}_{c, \lambda} = \{(x_c, y_c, z_c) : ((x_v, y_v, z_v))_{v \in V_H} \in S_{\mathbb{R}}(H, \lambda, v_1v_2v_3)\}$$

is called a coupler curve of c w.r.t. the fixed triangle $v_1v_2v_3$.

Assuming that a coupler curve is fixed, i.e., we have fixed lengths λ of the graph H , we can change the edge length λ_{uc} so that the number of intersections of the coupler curve $\mathcal{C}_{c, \lambda}$ with the sphere with the center at u and radius λ_{uc} , namely, the number of real embeddings of G , is maximal.

The following lemma shows that we can change three more edge lengths within one parameter family without changing the coupler curve. This one parameter family corresponds to shifting the center of the sphere along a line.

Lemma 2. Let $G = (V, E)$ be a minimally rigid graph and u, v, w, p, c be vertices of G such that $pv, vw \in E$ and the neighbours of u in G are v, w, p and c . Let H be the graph given by $(V_H, E_H) = (V, E \setminus \{uc\})$ with generic edge lengths $\lambda = (\lambda_e)_{e \in E_H}$. Let $\mathcal{C}_{c, \lambda}$ be the coupler curve of c w.r.t. the fixed triangle vuw . Let z_p be the altitude of p in the triangle uwp with lengths given by λ . Then the set $\{y_p : ((x_{v'}, y_{v'}, z_{v'}))_{v' \in V_H} \in S_{\mathbb{R}}(H, \lambda, vuw)\}$ has only one element y'_p . If the

parametric edge lengths $\lambda'(t)$ are given by

$$\begin{aligned}\lambda'_{uw}(t) &= \|(x_w, y_w - t, 0)\|, & \lambda'_{up}(t) &= \|(0, y'_p - t, z_p)\|, \\ \lambda'_{uv}(t) &= t, \text{ and } \lambda'_e(t) = \lambda_e \text{ for all } e \in E_H \setminus \{uv, uw, up\},\end{aligned}$$

then the coupler curve $\mathcal{C}_{c, \lambda'(t)}$ of c w.r.t. the fixed triangle vuw is the same for all $t \in \mathbb{R}_+$, namely, it is $\mathcal{C}_{c, \lambda}$. Moreover, if $cw \in E$, then $\mathcal{C}_{c, \lambda}$ is a spherical curve.

Proof. All coupler curves in the proof are w.r.t. the triangle vuw . Figure 6 illustrates the statement. Since G is minimally rigid, the set $S_{\mathbb{R}}(H, \lambda, vuw)$ is 1-dimensional. The coupler curve $\mathcal{C}_{p, \lambda}$ of p is a circle whose axis of symmetry is the y -axis. Hence, the set $\{y_p : ((x_{v'}, y_{v'}, z_{v'}))_{v' \in V_H} \in S_{\mathbb{R}}(H, \lambda, vuw)\}$ has indeed only one element. The parametrized edge lengths $\lambda'(t)$ are such that the position of v and w is the same for all t . Moreover, the coupler curve $\mathcal{C}_{p, \lambda'(t)}$ of p is independent of t . Hence, the coupler curve $\mathcal{C}_{c, \lambda'(t)}$ is independent of t , because the only vertices adjacent to u in H are p, v and w . Thus, the positions of the other vertices are not affected by the position of u . \square

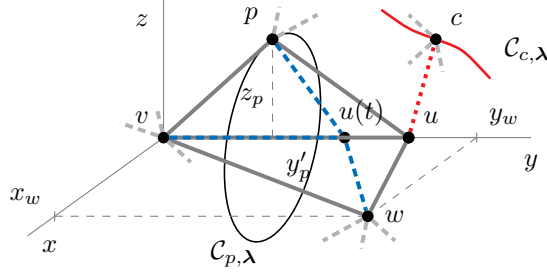


Figure 6: Since the lengths of up and uw are changed accordingly to the length of uv (blue dashed edges), the coupler curves $\mathcal{C}_{p, \lambda'(t)}$ and $\mathcal{C}_{c, \lambda'(t)}$ are independent of t . The red dashed edge uc is removed from G .

Therefore, for every subgraph of G induced by vertices u, v, w, p, c such that $\deg(u) = 4$ and $pv, vw, uv, uw, up, uc \in E$, we have a 2-parametric family of lengths $\lambda(t, r)$ such that the coupler curve $\mathcal{C}_{c, \lambda(t, r)}$ w.r.t. the fixed triangle vuw is independent of t and r . Recall that the parameter r represents the length of uc , which corresponds to the radius of the sphere, and the parameter t determines the lengths of uv, uw and up . Now, we aim to find r and t such that $r_3(G, \lambda(t, r))$ is maximized.

Let us clarify that whereas [7] were changing the coupler curve, our approach is different in the sense that the coupler curve is preserved within one step of our method, while the position and radius of the sphere corresponding to the removed edge are changed in order to have as many intersections as possible. In the next step, we pick a different edge to be removed. We discuss in Section 3.2.2, how these steps are combined for various subgraphs.

In order to illustrate the method, let λ be edge lengths of G_{48} given by

$$\begin{aligned}\lambda_{12} &= 1.99993774567597, & \lambda_{27} &= 10.5360917228793, & \lambda_{23} &= 0.99961432208948, \\ \lambda_{13} &= 1.99476987780024, & \lambda_{37} &= 10.5363171636461, & \lambda_{34} &= 1.00368644488060, \\ \lambda_{14} &= 2.00343646098439, & \lambda_{47} &= 10.5357233031495, & \lambda_{45} &= 1.00153014850485, \\ \lambda_{15} &= 2.00289249524296, & \lambda_{57} &= 10.5362736599978, & \lambda_{56} &= 0.99572361653574, \\ \lambda_{16} &= 2.00013424746814, & \lambda_{67} &= 10.5364788463527, & \lambda_{26} &= 1.00198771097407.\end{aligned}$$

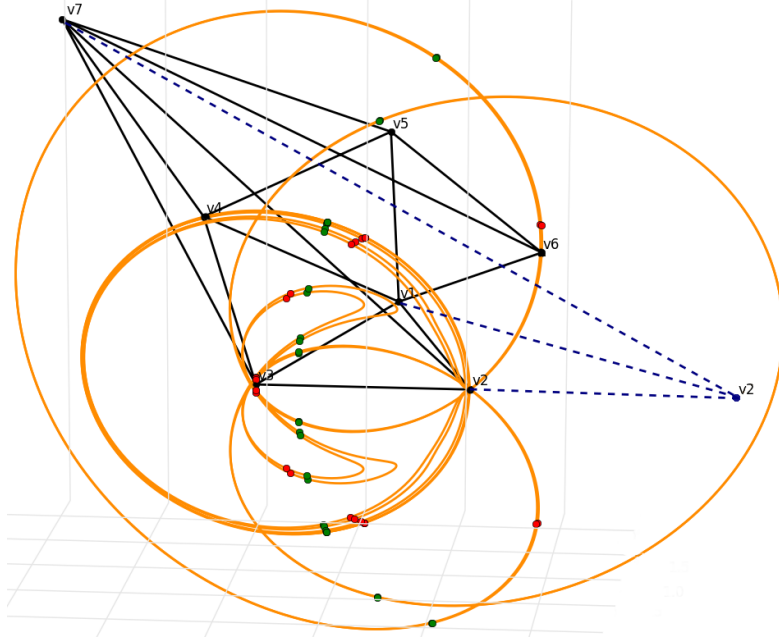


Figure 7: The coupler curve $\mathcal{C}_{v_6, \lambda}$ of G_{48} with the edge v_2v_6 removed. The 28 red points are intersections of $\mathcal{C}_{v_6, \lambda}$ with the sphere centered at v_2 with the edge lengths λ , whereas the 32 green ones are for the adjusted edge lengths (illustrated by blue dashed lines).

Using `Matplotlib` by [19], our program [2] can plot the coupler curve of the vertex v_6 of the graph $G_{48} - v_2v_6$ w.r.t. the fixed triangle $v_1v_2v_3$, see Figure 7 for the output. There are 28 embeddings for λ . Following Lemma 2 for the subgraph given by $(u, v, w, p, c) = (v_2, v_3, v_1, v_7, v_6)$, one can find a position and radius of the sphere corresponding to the removed edge v_2v_6 such that there are 32 intersections. Such edge lengths are obtained by taking $\lambda_{12} = 4.0534$, $\lambda_{27} = 11.1069$, $\lambda_{26} = 3.8545$, $\lambda_{23} = 4.0519$.

3.2.1 Sampling procedure

Instead of finding suitable parameters for the position and radius of the sphere by looking at visualizations, we implemented a sampling procedure that tries to maximize the number of intersections [2]. Whereas the version presented at ISSAC'18 worked only for a short list of predefined graphs, the current one takes an arbitrary minimally rigid graph containing a triangle. The inputs of the function `sampleToGetMoreEmbd` are starting edge lengths λ and vertices u, v, w, p, c satisfying the assumptions of Lemma 2, including the extra requirement that cw is an edge. For simplicity, we identify vertices with their positions in \mathbb{R}^3 and edges with the corresponding lines in the explanation of the procedure.

Let S_u be the sphere centered at u representing the removed edge uc . The extra assumption that cw is an edge is useful since then the coupler curve lies in a sphere S_w centered at w . Hence, the intersections of the coupler curve of c with S_u are on the intersection $S_u \cap S_w$, which is a circle. Thus, we can sample circles on the sphere S_w instead of sampling the parameters t and r .

The center of the intersection circle $S_u \cap S_w$ is on the line uw , which is perpendicular to the plane of the circle. Hence, the circle is determined by the angle $\varphi \in (-\pi/2, \pi/2)$ between

the altitude of w in the triangle uvw and the line uw , and by the angle $\theta \in (0, \pi)$ between uw and cw , see Figure 8. Clearly, the lengths of uv, uw, up and uc are defined uniquely by the pair (φ, θ) and the other edge lengths. Thus, we sample φ and θ in their intervals instead of sampling the parameters r and t . An advantage of this approach is that φ and θ are in bounded intervals, whereas t and r are unbounded. Moreover, sampling the angles uniformly gives a more reasonable distribution of the intersection circles on the sphere S_w than the uniform sampling of t and r .

Since for every sample we have to solve a system of equations in order to count the number of real embeddings, we exploit the following strategy to decrease the number computations: In the first phase, we sample both angles at approximately 20–24 points each and we take the pairs (φ, θ) attaining the maximum number. In the second phase, we sample few more points around each of these pairs to have a finer sampling in relevant areas. Of course, edge lengths with the maximum number of real embeddings are outputted.

The homotopy continuation package `phcpy` by [32] is used for solving the algebraic systems. A significant speedup of the computation is achieved by tracking the solutions from a previous system, instead of solving the system every time from scratch. Besides the fact that `phcpy` is parallelized, our implementation splits the samples into two parts and computes the numbers of embeddings for them in parallel.

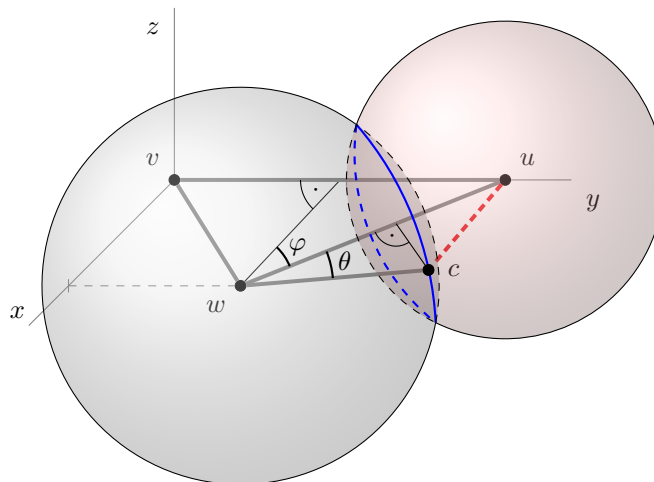


Figure 8: For fixed position of v and w , the angle φ determines the position of u , since u lies on the y -axis. If also the length of cw is given, then θ determines the length of uc . The intersection circle is blue.

3.2.2 More subgraphs suitable for sampling

It is likely that the sampling procedure for one choice of (u, v, w, p, c) does not yield the number of real embeddings that matches the complex bound. Hence, we repeat the procedure for various choices of (u, v, w, p, c) , assuming that there are more subgraphs satisfying the conditions of Lemma 2.

If the sampling procedure produces more edge lengths with the same number of real embeddings, then we need to select starting edge lengths for sampling with a different subgraph, since

it is not computationally feasible to test all of them.

We use a heuristic based on clustering of pairs (φ, θ) corresponding to the edge lengths by the function `DBSCAN` from `sklearn` package [25]. We take either the edge lengths belonging to the center of gravity of each cluster, or the pair (φ, θ) closest to this center if the edge lengths corresponding to the center have a lower number of real embeddings.

We propose two different approaches for iterating the sampling procedure for various subgraphs. The first one, called *tree search*, applies the sampling procedure using all suitable subgraphs for a given λ . Then, the same is done recursively for all output edge lengths whose number of real embeddings increased. The state tree is traversed depth-first, until the required number of real embeddings is reached (or there are no increments). This algorithm is implemented in the function `findMoreEmbeddings_tree` in our code.

The function `findMoreEmbeddings` uses the second approach, called *linear search*. Assume an order of the suitable subgraphs. The output from the sampling procedure applied to starting edge lengths with the first subgraph is the input for the procedure with the second subgraph, etc. The output from the last subgraph is used again as the input for the first one. There is also a branching because of multiple clusters — all of them are tested in depth-first way. Again, we stop either if the required number of real embeddings is reached, or there all the subgraphs are used without increment of the number of real embeddings.

For both, the subgraphs to be used can be specified, or the program computes all suitable subgraphs by itself. Tree search is useful when one wants to find subgraphs whose application leads to the desired number of embeddings in the least number of iterations. On the other hand, linear search seems more efficient. We remark that there is also an option to relax the condition that $\deg(u) = 4$. Then, such a subgraph can also be used for sampling, but the coupler curve changes during the process.

4 Classification and Lower Bounds

The first step of our procedure was to construct Laman and Geiringer graphs by Henneberg steps. We subsequently removed isomorphic duplicates and classified them according to the last Henneberg move as described in Section 2.1. Following an idea explained in [18], we represented every graph isomorphism class with an integer and we proceeded using a `SageMath` implementation.

A first upper bound on the number of embeddings is the mixed volume of systems of sphere and distance equations. This bound is crucial for homotopy continuation system solving, as mentioned before. The second natural bound of graph realizations is the number of complex embeddings. The numbers of complex embeddings for all Laman graphs up to 12 vertices are known from [8], while the numbers of complex embeddings of Geiringer graphs up to 10 vertices were computed by [18]. We computed the complex solutions of spherical embeddings of Laman graphs up to 8 vertices. For the last part, we were motivated by a remark of Josef Schicho, who observed that the numbers of planar and spherical solutions differ for the Desargues graph.

In order to find parameters that can maximize the number of real embeddings, we applied the methods described in Section 3. Polynomial system solving during sampling was accomplished mainly via `phcpy`. We consider an embedding being real if the absolute value of the imaginary part of every coordinate is less than 10^{-15} . The final results were verified using Maple's `RootFinding` [Isolate]. Our results ameliorate significantly what was known about the bounds of real embeddings.

4.1 Laman Graphs

The numbers of realizations of all 6-vertex Laman graphs are known [7]. There are four H2-last Laman graphs and the upper bound of real embeddings was computed in [12] for the graph with the maximal number of complex embeddings. Using stochastic and parametric methods, we were also able to maximize the number of embeddings for the other three 7-vertex graph with not trivial number of embeddings, completing a full classification for all 7-vertex Laman graphs according to their number of real embeddings [2].

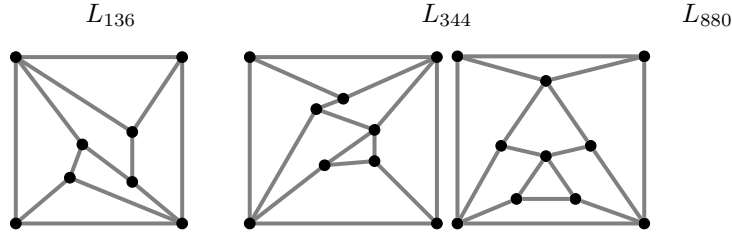


Figure 9: Laman graphs with maximal numbers of complex embeddings with $8 \leq n \leq 10$. We have found tight bounds for $n = 8$ and $n = 9$.

For bigger graphs, we focused on the graphs with the maximal number of complex embeddings, see Figure 9. The following table summarizes the bound on $r_2(G)$. Notice that it shows that there exist edge lengths such that all embeddings of the 8-vertex graph L_{136} and of the 9-vertex graph L_{344} are real.

n	8	9	10
	L_{136}	L_{344}	L_{880}
MV sphere eq.	192	512	1536
MV distance eq.	136	344	880
$c_2(G)$	136	344	880
$r_2(G) \geq$	136	344	860*

Now, we provide edge lengths giving the numbers of real embeddings in the table.

L_{136} :	$\lambda_{1,2} = 1.000109994$,	$\lambda_{1,4} = 1.000334944$,	$\lambda_{1,8} = 1.000119993$,
$\lambda_{2,3} = 1.000174985$,	$\lambda_{2,7} = 1.000379928$,	$\lambda_{3,6} = 1.000459894$,	$\lambda_{3,8} = 1.000099995$,
$\lambda_{4,5} = 1.000049999$,	$\lambda_{4,7} = 1.000144989$,	$\lambda_{5,7} = 1.000389924$,	$\lambda_{5,8} = 1.000354937$,
$\lambda_{6,7} = 1.000244970$,	$\lambda_{6,8} = 1.000289958$,		
L_{344} :	$\lambda_{1,4} = 1.00100$,	$\lambda_{1,6} = 1.00046$,	$\lambda_{1,9} = 1.00057$,
$\lambda_{2,3} = 1.00058$,	$\lambda_{2,5} = 1.00075$,	$\lambda_{2,8} = 1.00084$,	$\lambda_{3,7} = 1.00073$,
$\lambda_{3,9} = 1.00042$,	$\lambda_{4,7} = 1.00096$,	$\lambda_{4,9} = 1.00015$,	$\lambda_{5,7} = 1.00083$,
$\lambda_{5,8} = 1.00003$,	$\lambda_{6,7} = 1.00086$,	$\lambda_{6,8} = 1.00008$,	$\lambda_{8,9} = 1.00039$,
L_{880} :	$\lambda_{1,4} = 1.0002169$,	$\lambda_{1,8} = 1.0001366$,	$\lambda_{1,10} = 1.0004509$,
$\lambda_{2,3} = 1.000763$,	$\lambda_{2,7} = 1.0000575$,	$\lambda_{2,10} = 1.0006078$,	$\lambda_{3,7} = 1.0001763$,
$\lambda_{3,9} = 1.00075$,	$\lambda_{4,8} = 1.0008574$,	$\lambda_{4,9} = 1.000536$,	$\lambda_{5,7} = 1.000491$,
$\lambda_{5,8} = 1.0002946$,	$\lambda_{5,10} = 1.0006778$,	$\lambda_{6,7} = 1.0004699$,	$\lambda_{6,8} = 1.0002724$,
$\lambda_{6,9} = 1.0005141$,	$\lambda_{9,10} = 1.0003913$,		

We shall note that while `phcpy` gives 868 real solutions for L_{880} , we were able to verify only 860 of them using Maple's `RootFinding [Isolate]` function for distance systems (sphere equations computation did not terminate in that case). The number of real solutions of distance systems was exactly the same as expected by the `phcpy` computation, but in some cases triangular inequalities were violated. The violation error was smaller than 10^{-8} . Although there is a strong possibility that this error is insignificant, we take that $r_2(L_{880}) \geq 860$.

Spherical embeddings of Laman graphs

Maximal numbers of embeddings in S^2 have been not studied so far. We attempted to find edge lengths such that the number of realizations was the same as the number of complex solutions for graphs that do not have a trivial number of embeddings. We shall observe again that the $c_2(G)$ varies for certain graphs from $c_{S^2}(G)$.

We have found parameters such that all the embeddings are real for all H2-last graphs with 6 and the 7-vertex graphs with the maximal number of complex embeddings (they can be found in [2]). The Desargues graph has the maximal number of embeddings among 6-vertex graphs, namely, it can have 32 realizations (instead of 24 on the plane). In the 7-vertex case, there are two H2-last graphs with 64 realizations (instead of 48 and 56 respectively on the plane), see Figure 10. Let us indicate that 64 realizations can be also achieved by the 3 graphs constructed by applying an H1 move on L_{24} , since H1 doubles the number of embeddings. Observe that this contrasts the situation of the complex embeddings in the plane, since it is known that for $n \leq 12$ there is always a unique Laman graph with the maximal number of complex embeddings on the plane among n -vertex Laman graphs. We have also found edge lengths that maximize the spherical embeddings of L_{136} (see Figure 9). It has 192 real spherical embeddings. We remark that there is again another graph with 192 complex spherical embeddings, but we have found edge lengths with only 136 real spherical embeddings.

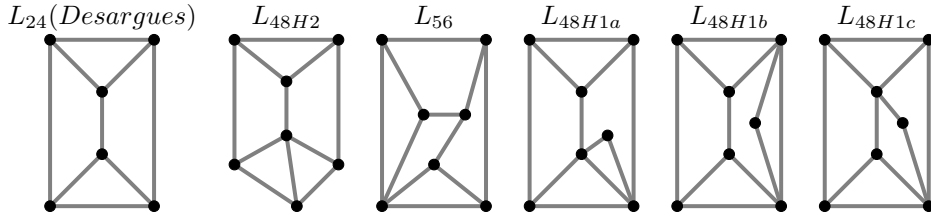


Figure 10: Laman graphs with maximal numbers of spherical embeddings with 6 vertices (L_{24} -Desargues graph with 32 spherical embeddings) and 7 vertices (L_{48H1a} , L_{48H1b} , L_{48H1c} , L_{48H2} and L_{56} -graphs with 64 spherical embeddings).

This table gives upper bound and the number of real spherical embeddings for all graphs with $6 \leq n \leq 8$ that have the maximal number of embeddings.

n	6	7	7	7	7	7	8
	L_{24}	L_{48H2}	L_{56}	L_{48H1a}	L_{48H1b}	L_{48H1c}	L_{136}
MV sphere eq.	32	64	64	64	64	64	192
MV distance eq.	32	64	64	64	64	64	192
$c_{S^2}(G)$	32	64	64	64	64	64	192
$r_{S^2}(G)$	32	64	64	64	64	64	192

We present a list of lengths (using euclidean metric) that give maximal number of realizations for the non-trivial (H2-last) cases:

L_{24} :	$\lambda_{1,2} = 1.43,$	$\lambda_{1,4} = 1.39,$	$\lambda_{1,6} = 1.055,$
	$\lambda_{2,3} = 1.45,$	$\lambda_{2,5} = 1.193,$	$\lambda_{3,4} = 1.388,$
	$\lambda_{4,6} = 1.691,$	$\lambda_{5,6} = 1.386,$	$\lambda_{3,5} = 1.64,$
L_{48H2} :	$\lambda_{1,2} = 1.526433752,$	$\lambda_{1,3} = 1.250599856,$	$\lambda_{1,4} = 1.519868415,$
	$\lambda_{2,5} = 1.772004515,$	$\lambda_{2,6} = 1.371860051,$	$\lambda_{2,7} = 1.019803903,$
	$\lambda_{3,7} = 1.363084737,$	$\lambda_{4,6} = 1.314534138,$	$\lambda_{5,6} = 1.754992877,$
			$\lambda_{6,7} = 1.054514106,$
L_{56} :	$\lambda_{1,2} = 1.921665944,$	$\lambda_{1,3} = 1.3,$	$\lambda_{1,5} = 1.337908816,$
	$\lambda_{2,5} = 1.058300524,$	$\lambda_{2,6} = 1.306139349,$	$\lambda_{2,7} = 1.468332387,$
	$\lambda_{3,7} = 0.6693280212,$	$\lambda_{4,5} = 1.370401401,$	$\lambda_{4,6} = 1.630337388,$
			$\lambda_{6,7} = 1.994993734.$
L_{136} :	$\lambda_{1,2} = 1.69431375697417,$	$\lambda_{1,5} = 1.53147820126884,$	$\lambda_{1,8} = 1.40741112578064,$
	$\lambda_{2,3} = 1.46514833488809,$	$\lambda_{2,5} = 1.43532284310132,$	$\lambda_{2,7} = 1.3673675423030,$
	$\lambda_{3,6} = 1.49080389256053,$	$\lambda_{4,5} = 1.36622835551227,$	$\lambda_{4,8} = 1.52724607627725,$
	$\lambda_{6,8} = 0.871783052046995,$	$\lambda_{7,8} = 1.76892528306539.$	$\lambda_{3,4} = 1.35543641920214,$
			$\lambda_{6,7} = 1.23765605522418.$

4.2 Geiringer graphs

The method we introduced in Section 3.2 played a crucial role in increasing the number of embeddings of Geiringer graphs. We used our method for the only H2-last graph with 6 vertices — the cyclohexane G_{16} . It was known that $r_3(G_{16}) = 16$, a result that can be verified by our method within a few tries with random starting lengths.

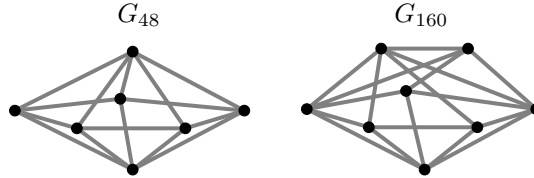


Figure 11: The 7-vertex and 8-vertex graphs with the maximal number of embeddings (G_{48} and G_{160}).

The case of $n = 7$ was the first open one. There are twenty H1-last 7-vertex Geiringer graphs and six H2-last ones. We computed the mixed volumes and the number of complex embeddings for each one of them. Then, using our code we were able to find edge lengths that give a full classification of all 7-vertex Geiringer graphs according to $r_3(G)$ [2].

We want to remark again at this point that G_{48} was the model for our coupler curve method. Using our implementation, we were able to find lengths that maximize the number of embeddings only after a few iterations. The structure of this graph fits perfectly to our method, since there are 20 subgraphs of G_{48} given by vertices (u, v, w, p, c) satisfying the assumption in Lemma 2.

Using tree search approach, we obtained edge lengths λ such that $r_3(G_{48}, \lambda) = 48$:

$$\begin{array}{llll} \lambda_{1,2} = 1.9999, & \lambda_{1,6} = 2.0001, & \lambda_{4,5} = 7.0744, & \lambda_{4,7} = 11.8471, \\ \lambda_{1,3} = 1.9342, & \lambda_{2,6} = 1.0020, & \lambda_{5,6} = 4.4449, & \lambda_{5,7} = 11.2396, \\ \lambda_{1,4} = 5.7963, & \lambda_{2,3} = 0.5500, & d_{2,7} = 10.5361, & \lambda_{6,7} = 10.5365, \\ \lambda_{1,5} = 4.4024, & \lambda_{3,4} = 5.4247, & \lambda_{3,7} = 10.5245, & \end{array}$$

They can be found from the starting edge lengths given in Sec. 3.2 with 28 real embeddings in only 3 iterations, using the subgraphs $(v_5, v_6, v_1, v_7, v_4)$, $(v_4, v_3, v_1, v_7, v_5)$ and $(v_3, v_2, v_1, v_7, v_4)$.

We repeated the same procedure for $n = 8$. In that case we can use the H1 doubling property for 311 graphs, while there are 63 graphs with a non-trivial number of embeddings. We computed complex bounds for all H2-last graphs [2]. We subsequently found edge lengths that increase the number of real embeddings of G_{160} , which is the graph with the maximal number of complex embeddings $c_3(G_{160}) = 160$. We were able to find parameters λ such that $r_3(G_{160}, \lambda) = 132$.

The following lengths give 132 real embeddings for G_{160} :

$$\begin{array}{llll} \lambda_{1,2} = 1.999, & \lambda_{2,3} = 1.426, & \lambda_{3,7} = 10.447, & \lambda_{5,8} = 4.279, \\ \lambda_{1,3} = 1.568, & \lambda_{2,6} = 0.879, & \lambda_{4,5} = 7.278, & \lambda_{6,8} = 0.398, \\ \lambda_{1,4} = 6.611, & \lambda_{2,7} = 10.536, & \lambda_{4,7} = 11.993, & \lambda_{7,8} = 10.474, \\ \lambda_{1,5} = 4.402, & \lambda_{2,8} = 0.847, & \lambda_{5,6} = 4.321, & \\ \lambda_{1,6} = 1.994, & \lambda_{3,4} = 6.494, & \lambda_{5,7} = 11.239, & \end{array}$$

We shall remark that our results about 7-vertex graphs and G_{160} appeared already in [1]. One may find a full list of Geiringer graphs with 7 and 8 vertices in [2]. Finally, we also want to notice that for all planar (in the graph-theoretical sense) Geiringer graphs up to 10 vertices, the number of complex embeddings is always equal to the mixed volume of the sphere equations system. A possible conjecture could be that mixed volume is tight for all planar Geiringer graphs.

4.3 Lower bounds

The maximal numbers of real embeddings that we found can serve to build an infinite class of bigger graphs. These frameworks can give us lower bounds on the maximum number of embeddings. To compute the lower bound, we will use the following theorem that combines caterpillar, fan and generalized fan constructions [18]:

Theorem 3. *Let $G = (V_G, E_G)$ be a generically rigid graph, with a generically rigid subgraph $H = (V_H, E_H)$. We construct a rigid graph using k copies of G , where all the copies have the subgraph H in common. The new graph is rigid, has $n = |V_H| + k(|V_G| - |V_H|)$ vertices, and the number of its real embeddings is at least*

$$2^{(n-|V_H|) \bmod (|V_G|-|V_H|)} \cdot r_d(H) \cdot \left(\frac{r_d(G)}{r_d(H)} \right)^{\left\lfloor \frac{n-|V_H|}{|V_G|-|V_H|} \right\rfloor}.$$

Remind that for a triangle T we have that $r_2(T) = r_{S^2}(T) = 2$, while $r_3(T) = 1$. For Laman graphs, the best asymptotic bound is derived from L_{880} :

Corollary 1. *The maximum number of real embeddings on the plane among Laman graphs with n vertices is bounded from below by*

$$2^{(n-3) \bmod 7} \cdot 2 \cdot 430^{\lfloor (n-3)/7 \rfloor}.$$

The bound asymptotically behaves as 2.378^n .

The previous lower bound in that case was 2.3003^n by [12].

In the case of spherical embeddings, we may use L_{24} :

Corollary 2. *The lower bound for the maximum number of spherical embeddings among Laman graphs with n vertices is*

$$2^{(n-3) \bmod 7} \cdot 2 \cdot 16^{\lfloor (n-3)/3 \rfloor}.$$

This bound asymptotically behaves as 2.51984^n .

We remark that L_{48H1a} , which has the 4-vertex Laman graph as a subgraph, can give the same asymptotic lower bound. The other 7-vertex graphs with $r_{S^2}(L) = 64$ can give only 2.3784^n as a lower bound, while the asymptotic bound from 8-vertex graph with 192 embeddings is 2.4914^n .

Finally, using the fact that $r_3(G_{160}) \geq 132$, we obtain the following result, which appeared also in [1]:

Corollary 3. *The maximum number of real embeddings of Geiringer graphs with n vertices can be bigger than*

$$2^{(n-3) \bmod 5} 132^{\lfloor (n-3)/5 \rfloor},$$

indicating that $r_3(n) \in \Theta(2.6553^n)$.

The previous lower bound for Geiringer graphs was 2.51984^n [14]. Using the graph G_{48} yields $r_3(n) \in \Theta(2.6321^n)$. Notice that we use a subgraph with one embedding and not with two, as we did in the cases of Laman graphs. This happens because there is no tetrahedron as a subgraph of the 8-vertex graphs that could give a better lower bound.

5 Conclusion and future work

In this paper we have developed and used efficient methods to maximize the number of real embeddings of rigid graphs in the case of planar, spherical and spatial embeddings. We have introduced a new technique for Geiringer graphs, that exploits an invariance property of coupler curves to select the sampling parameters at each iteration. This procedure led to classification results and to an improvement of the asymptotic lower bounds.

As future work, a first goal would be to ameliorate the maximal real bounds in all cases. It is an interesting question if we can develop a similar sampling technique, as the one we introduce in this paper, for other cases and/or other structures of Geiringer graphs. Besides lower bounds, it is believed that upper bounds are really loose, so an open problem is to improve them in the general case or for specific classes of graphs.

Acknowledgments This work is part of the project ARCADES that has received funding from the European Union's Horizon 2020 research and innovation programme under the Marie Skłodowska-Curie grant agreement No 675789. ET is partially supported by ANR JCJC GALOP (ANR-17-CE40-0009) and the PGMO grant GAMMA.

References

- [1] E. Bartzos, I.Z. Emiris, J. Legerský, and E. Tsigaridas. On the Maximal Number of Real Embeddings of Spatial Minimally Rigid Graphs. In *Proceedings of the 2018 ACM International Symposium on Symbolic and Algebraic Computation, ISSAC '18*, pages 55–62, New York, NY, USA, 2018. ACM.

- [2] E. Bartzos and J. Legerský. Graph embeddings in the plane, space and sphere — source code and results. Zenodo, 2018.
- [3] F. Bihan, J. M. Rojast, and F. Sottile. On the sharpness of fewnomial bounds and the number of components of fewnomial hypersurfaces. In *Algorithms in algebraic geometry*, pages 15–20. Springer, 2008.
- [4] Frédéric Bihan, Francisco Santos, and Pierre-Jean Spaenlehauer. A polyhedral method for sparse systems with many positive solutions. *arXiv preprint arXiv:1804.05683*, 2018.
- [5] L. M. Blumenthal. *Theory and Applications of Distance Geometry*. Chelsea Publishing Company, New York, 1970.
- [6] C. S. Borcea. Point configurations and Cayley-Menger Varieties. *arXiv:math/0207110*, 2002.
- [7] C. S. Borcea and I. Streinu. The Number of Embeddings of Minimally Rigid Graphs. *Discrete & Computational Geometry* 2, page 287–303, 2004.
- [8] J. Capco, M. Gallet, G. Grasegger, C. Koutschan, N. Lubbes, and J. Schicho. The Number of Realizations of a Laman Graph. *SIAM Journal on Applied Algebra and Geometry*, 2(1):94–125, 2018.
- [9] R. Connelly. Generic global rigidity. *Discrete Comput. Geom.* 33, page 549–563, 2005.
- [10] M. Dattorro and J. Dattorro. Convex Optimization & Euclidean Distance Geometry, 2005.
- [11] P. Dietmaier. The Stewart-Gough platform of general geometry can have 40 real postures. *Advances in Robot Kinematics: Analysis and Control*, pages 1–10, 1998.
- [12] I. Z. Emiris and G. Moroz. The assembly modes of rigid 11-bar linkages. *IFToMM 2011 World Congress, Jun 2011, Guanajuato, Mexico*, 2011.
- [13] I. Z. Emiris and B. Mourrain. Computer Algebra Methods for Studying and Computing Molecular Conformations. *Algorithmica* 25, pages 372–402, 1999.
- [14] I.Z. Emiris, E. Tsigaridas, and A. Varvitsiotis. Mixed volume and distance geometry techniques for counting Euclidean embeddings of rigid graphs. *Distance Geometry: Theory, Methods and Applications*, edited by A. Mucherino, C. Lavor, L. Liberti and N. Maculan, pages 23–45, 2013.
- [15] D.G. Emmerich. *Structures Tendues et Autotendantes*. Ecole d’Architecture de Paris la Villette, 1988.
- [16] J.C. Faugère and D. Lazard. The combinatorial classes of parallel manipulators. *Mechanism & Machine Theory* 30(6), pages 765–776, 1995.
- [17] S. Gortler, A. Healy, and D. Thurston. Characterizing generic global rigidity. *Am. J. Math.* 132(4), pages 897–939, 2010.
- [18] G. Grasegger, C. Koutschan, and E. Tsigaridas. Lower Bounds on the Number of Realizations of Rigid Graphs. *Experimental Mathematics*, pages 1–12, 2018.
- [19] J. D. Hunter. Matplotlib: A 2D graphics environment. *Computing In Science & Engineering*, 9(3):90–95, 2007.

- [20] B. Jackson and J.C. Owen. Equivalent Realisations of Rigid Graphs. *10th Japanese-Hungarian Symposium on Discrete Mathematics and Its Applications*, pages 283–289, 2017.
- [21] B. Jackson and J.C. Owen. Equivalent realisations of a rigid graph. *Discrete Applied Mathematics*, 2018.
- [22] G. Laman. On graphs and rigidity of plane skeletal structures. *Journal of Engineering Mathematics*, 4(4):331–340, Oct 1970.
- [23] L. Liberti, B. Masson, J. Lee, C. Lavor, and A. Mucherino. On the number of realizations of certain Henneberg graphs arising in protein conformation. *Discrete Applied Mathematics*, 165, page 213–232, 2014.
- [24] J.C. Maxwell. On the calculation of the equilibrium and stiffness of frames. *Philosophical Magazine*, page 39(12), 1864.
- [25] F. Pedregosa, G. Varoquaux, A. Gramfort, V. Michel, B. Thirion, O. Grisel, M. Blondel, P. Prettenhofer, R. Weiss, V. Dubourg, J. Vanderplas, A. Passos, D. Cournapeau, M. Brucher, M. Perrot, and E. Duchesnay. Scikit-learn: Machine Learning in Python. *Journal of Machine Learning Research*, 12:2825–2830, 2011.
- [26] H. Pollaczek-Geiringer. Über die Gliederung ebener Fachwerke. *Zeitschrift für Angewandte Mathematik und Mechanik (ZAMM)*, 7(1):58–72, 1927.
- [27] H. Pollaczek-Geiringer. Zur Gliederungstheorie räumlicher Fachwerke. *Zeitschrift für Angewandte Mathematik und Mechanik (ZAMM)*, 12(6):369–376, 1932.
- [28] B. Schulze and W. Whiteley. *Rigidity and scene analysis*, chapter 61, pages 1593–1632. CRC Press LLC, 2017.
- [29] F. Sottile. Enumerative real algebraic geometry. In *Algorithmic and Quantitative Real Algebraic Geometry, DIMACS Series in Discrete Mathematics and Theoretical Computer Science, Volume 60*, AMS, pages 139–180, 2003.
- [30] R. Steffens and T. Theobald. Mixed volume techniques for embeddings of Laman graphs. *Computational Geometry* 43, pages 84–93, 2010.
- [31] T.-S. Tay and W. Whiteley. Generating isostatic frameworks. *Topologie Structurale*, pages 21–69, 1985.
- [32] J. Verschelde. Modernizing PHCpack through phcpy. In *Proceedings of the 6th European Conference on Python in Science (EuroSciPy 2013)*, pages 71–76, 2014.
- [33] D. Walter and M. L. Husty. On a 9-bar linkage, its possible configurations and conditions for paradoxical mobility. *IFTToMM World Congress, Besançon, France*, 2007.
- [34] W. Whiteley. Cones, infinity and one-story buildings. *Topologie Structurale*, 8:53–70, 1983.
- [35] D. Zelazo, A. Franchi, F. Allgöwer, H. H. Bühlhoff, and P.R. Giordano. Rigidity Maintenance Control for Multi-Robot Systems. *Robotics: Science and Systems, Sydney, Australia*, 2012.
- [36] Z. Zhu, A.M.-C. So, and Y. Ye. Universal rigidity and edge sparsification for sensor network localization. *SIAM Journal on Optimization*, 20(6), page 3059–3081, 2010.